NASA Technical Memorandum 108798

Development of Lightweight Ceramic Ablators and Arc-Jet Test Results

Huy K. Tran

January 1994

National Aeronautics and
Space Administration

Ames Research Center
Moffett Field, California 94035-1000

Development of Lightweight Ceramic Ablators and Arc-Jet Test Results

HUY K. TRAN

Ames Research Center

Summary

Lightweight ceramic ablators (LCAs) were recently developed at Ames to investigate the use of low density fibrous substrates and organic resins as high temperature, high strength ablative heat shields. Unlike the traditional ablators, LCAs use porous ceramic/carbon fiber matrices as substrates for structural support, and polymeric resins as fillers. Several substrates and resins were selected for the initial studies, and the best performing candidates were further characterized. Substrates used in this experiment include the flight certified reusable surface insulation (RSI) such as Lockheed Insulation-900 (LI-900), the Ames developed alumina enhanced thermal barriers (AETB-20 and AETB-50), and Fiber Materials Inc. (FMI) carbon Fiberform® insulation. Methylmethacrylate (pmma), epoxy, and phenolic were selected as infiltrants with char yields ranging from 0 to 61%.

Three arc-jet tests were conducted to determine the LCA's thermal performance and ablation characteristics in a high enthalpy, hypersonic flow environment. Phases I and III were conducted in the 60 MW Interactive Heating Facility (IHF) where the cold wall heat heating rates ranged from 830 to 1,440 Btu/ft^2-sec and stagnation pressures of 0.081 to 0.333 atm. Phase II was performed in the 20 MW Aerodynamic Heating Facility (AHF) where the cold wall heating rates ranged from 100 to 400 Btu/ft^2-sec and pressures from 0.018 to 0.062 atm. Mass loss and recession measurements were obtained for each sample at post test, and the recession rates were determined from high speed motion films. Surface temperatures were also obtained from optical pyrometers.

Introduction

Future space vehicles such as Mars Environmental Survey (MESUR) and other proposed manned exploration of other interstellar planets will experience severe heat loads during descent into planet's orbit (ref. 1). These vehicles will require heat shields that can protect the vehicles from both high radiative heating environment and high shear load. In the past decades, several conventional ablative heat shields such as Avcoat 5206-HC and SLA-561 were developed for the Apollo and Viking missions. These ablators were effective in protecting the vehicles from the high heating environment. But because of their high density, however, these materials are not always mass efficient. It is important to reduce the total TPS weight of the vehicle as a way to maximize scientific payload.

The objective of this report is to describe the development and fabrication of LCAs and the results of preliminary thermal performance analysis obtained from arc-jet testing. LCAs use the low density porous fiber matrix that is partially impregnated with polymeric resin. Special infiltration techniques were developed to control the amount of resins so that the final product maintains the high porosity and low thermal conductivity. With the new impregnation techniques, LCAs can be produced which have very low density. This is believed to be mass efficient as a technique to economize on structural weight and fuel. Materials analyses consist of thermogravimetric analysis (TGA), elemental analysis of char, and ablation characteristics in a high enthalpy, hypersonic environment. A general infiltration technique of polymeric resins in ceramic substrates is described, and materials properties' measurements are discussed. Several conventional ablators such as Avcoat-5026-HC, SLA-561, ACUSIL-1, and MA-25S as well as balsa wood (ref. 2) were also evaluated for direct comparison purposes.

I would like to thank the following individuals for their contributions to this project: Daniel J. Rasky, Ming TA-Hsu, William Henline, Riccitiello Salvatore, Lili Esfahani, Angela Robinson, and Lynn Amon.

Materials

Table 1a shows material compositions and densities of different substrates and infiltrants used in the LCA's development. Special impregnation techniques and curing procedures were developed for each infiltrant. Three infiltrants were selected based on char yield, and four substrates were used based on their temperature capabilities and mechanical properties. LCAs were produced with two densities—15 lbm/ft^3 (partially dense where the amount of resin infiltrated in the matrix is

controlled) and 85 lbm/ft^3 (fully dense where the resin fills the entire porous volume). Two compositions of the AETB based LCAs (a-LCAs) were used to take advantage of the high melting temperature of alumina fibers (table 1). The silica based LCAs (s-LCAs) use the high purity microquartz fibrous LI-900 as substrates. Another silica substrate used in the LCA's development is the Ames Insulation-8 (AI-8) which consists of 98.5% microquartz fibers and 1.5% by weight of silicon carbide (SiC) powder (21 μm diameter particle size). The addition of SiC particles increases the AI-8's total hemispherical emittance and takes advantage of substrate reradiation as an additional way of rejecting heat at the surface.

The carbon based LCAs (c-LCAs) used carbon Fiberform® insulation manufactured by Fiber Materials, Inc. (FMI). The carbon Fiberform insulation is made of 14–16 μm diameter and 1,600 μm length carbon fibers which are bonded together with phenolic resin. Fiberform is a low density, rigid, carbon bonded carbon fiber insulation that can be used in a vacuum or inert environment at temperatures up to 5,460°R. Its density varies from 8.00 to 12.44 lbm/ft^3 (ref. 3). Another carbon material used in this study is the carbon-bonded carbon fiber (CBCF) material manufactured by Oak Ridge National Laboratory (ref. 4). CBCF was originally developed for use as a radioisotope heat source and is made of small diameter (10.5 μm) continuous rayon filaments that were precision chopped to 0.25 nm length. The fibers are then carbonized at 2,921°R and bonded with phenolic resin. The phenolic resin in the FMI Fiberform insulation was completely pyrolyzed to bond the carbon fibers, whereas the phenolic resin in CBCF is partially pyrolyzed and remains as particles within the fiber matrix.

Table 1b shows the composition, density of conventional ablators, and test conditions at which each sample was evaluated. Avcoat 5026-39HC and SLA-561 were developed and used as ablative heat shields for the Apollo and Viking spacecraft (ref. 5), respectively. Both materials have been flight certified, and this is the reason that they are used as a benchmark in the evaluation of LCA's performance. The MA-25S manufactured by Martin Marietta is a medium density ablator that has been used as a thermal protection material on the space shuttle external tank. It is an elastomeric silicone-based material that can be applied by spraying or molding at room temperature (ref. 6). The Acusil-1 is manufactured by Acurex Corporation and will be used as thermal protection on the COMET probe (ref. 7).

Infiltration Technique

Figure 1 shows a custom made apparatus for the infiltration process of LCA's test models. Each model is individually impregnated to ensure the uniform distribution of the resin within the ceramic matrix. The volume and density of each model are calculated from the weight, length, and diameter and are used to determine the amount of resin and solvent needed for the infiltration process. Different curing processes and drying procedures were developed for each resin. For example, after the substrate absorbs the pmma infiltrant as a resin solution, a 24-hour air dry is needed to complete the curing cycle and to evaporate the solvent. The phenolic infiltrant, on the other hand, requires a two-step curing process to ensure a complete cross linking of the polymer. This curing process requires several heating cycles and several days to complete the infiltration process.

Materials Testing and Analysis

It is necessary to obtain the thermophysical and thermochemical properties of LCAs in order to better describe and evaluate their thermal performance and ablation characteristics. Tests and analyses described in this paper were to be used as a screening process to select the best performing LCA candidates. Further characterizations are needed to fully understand the performance of each selected material as discussed below.

1. Thermogravimetric Analysis (TGA)

Thermogravimetric analysis gives the decomposition temperature and weight loss of each material as a function of temperature at a given constant heating rate. The pyrolysis rate constant and the char yield of polymers can also be determined from these data.

2. Gas Composition and Mass Spectroscopy (GCMS)

Elemental composition analysis of the char using GCMS was obtained for each resin used in LCAs.

3. High Enthalpy, Hypersonic Flow Environment

a. Facilities– Three arc-jet tests were conducted in two different arc-jet facilities located at NASA Ames Research Center—the 20 MW Aerodynamic Heating Facility (AHF) and the 60 MW Interactive Heating Facility (IHF). In general, an arc-jet facility, shown in figure 2, uses an electrical discharge to heat a gas stream to very high temperature. The result is a highly energetic

(i.e., high enthalpy) gas flow that can be used to create the aerothermodynamic heating conditions that are similar to re-entry flight environments experienced by a space vehicle. The test gas, which is air for the case of simulated earth re-entry, is heated by an electrical discharge confined within the 6-cm (20 MW AHF) or 8-cm (60 MW IHF) diameter constrictor column of the arc heater (ref. 8). After leaving the arc heater column, the highly energized gas is supersonically expanded by a convergent–divergent nozzle and is discharged into an evacuated test chamber where the test model is located. The stream velocity and enthalpy can be varied by using different nozzle exit to throat ratios. The area ratios can be varied from 64 to 400 in the 20 MW AHF and 8.6 to 298 in the 60 MW IHF. The stream can attain enthalpies up to 20,000 Btu/lbm and velocities up to Mach 8.

Stagnation point heat transfer rates and pressures were measured by copper calorimeter, and stagnation enthalpy was approximated using a nozzle flow computer code (ref. 9). Table 2a shows the nominal test conditions used in three test phases. Listed are the heat flux, stagnation pressure, estimated enthalpy, and model nose radius used in each test phase.

b. Test Models– Test models and holders were designed based on the constraints of heating requirements and are shown in figure 3. In Phase II, two of each s-LCA-m and s-LCA-p models were instrumented with type R thermocouples to obtain the in-depth temperature profiles as a function of exposure time.

c. Instrumentation– Optical pyrometers were used to estimate the model's surface temperature by adjusting the apparent brightness of the model during arc-jet exposure. This pyrometer was mounted outside the test box and viewed through a quartz window and was manually recorded. A Thermogage® pyrometer with a 30 in. focal length and wavelength of ~0.8 μm was mounted inside the test chamber. Figure 4 shows the setup of the pyrometer and motion film apparatus.

Experiment and Results

1. Thermogravimetric Analysis

Figure 5 shows the percentage of weight loss of three organic infiltrants from 23°C to 1,100°C at heating rate of 50° per minute in nitrogen environment. Decomposition temperature, T_d, was determined by using the intersect point of two tangent lines at the curvature. The initial stage of the decomposition process of phenolic occurs at 260°C, and the final stage is at 640°C where ~46% of its weight was removed. Similarly, the epoxy started to decompose at 330°C and lost ~78% of its weight at 600°C. Pmma's decomposition process is more dramatic; the process began at 350°C and completed at 600°C where almost all of pmma was removed. The char yield of each resin is determined by obtaining TGAs in both air and inert environment. Phenolic has the highest char yield (~61%) and pmma has the lowest (~0%); meanwhile, the char yield of epoxy is at midpoint (~23%).

TGAs of ceramic fiber matrix LCAs with and without the above resins did not show any changes in the decomposition temperatures and mass loss.

2. Gas Composition and Mass Spectroscopy (GCMS)

Table 2b shows the elemental composition of pmma, epoxy, and phenolic resins obtained from GCMS analysis. As expected, the char mainly consists of elemental carbon, some oxygen, and small amount of hydrogen.

3. Arc-Jet Test Results

Results are tabulated for each test phase and are grouped by materials and test conditions (i.e., heat flux, stagnation pressure, and exposure time). Density, weight, and length measurements were obtained for each sample at both pretest and posttest and are shown in tables 3, 4, and 5 for Phases I, II, and III, respectively.

The difference in density of each material can give a false representation of the recession data; thus, a new parameter is introduced to account for this nonuniformity (ref. 10). The mass loss flux is defined as the product of the stagnation recession rate and material's virgin density to account for the difference in density of the materials used in this experiment.

$$\dot{m} = \dot{s}\rho_v$$

The effective heat of ablation, H_{eff}, is calculated based on the measured recession rate, $\dot{s}$, and virgin density, ρ_v, of each material using the following equation:

$$H_{eff} = \frac{\dot{q}_{cw}}{\dot{s}\rho_v}$$

where $\dot{s}$ is the measured recession rate obtained from high speed films. H_{eff} can also be calculated using the mass loss rate and cold wall (cw) heat flux (ref. 11).

$$H_{eff} = \frac{\dot{q}_{cw}}{\dot{m}A}$$

where $\dot{m}$ is the total mass loss rate. The H_{eff} values presented in the last column of the tables are based on

the stagnation point recession rather than $\dot{m}$ because the mass loss values reported in tables 3–5 include the mass loss at both surface and side walls of the test models.

a. 60 MW IHF Phase I Test– Table 3 shows the test result of Phase I testing in the 60 MW IHF at two heat flux levels, 830 and 1,100 Btu/ft^2-s, with stagnation pressures of 0.081 and 0.141 atm, respectively. LCA's test models were produced with two densities, ~65 and ~14 lbm/ft^3. The following observations can be made from the Phase I testing.

(1) Fully Dense LCAs: As shown in figure 6, the mass loss fluxes of all high density LCAs are of the same order of magnitude. However, the test models with epoxy infiltrant suffered severe cracking at the tip and around the side walls. LCAs with pmma infiltrant (~0% char yield resin) had a thin layer of char (carbonaceous material) on the surface due to a phenomenon called molecular cracking. When pmma decomposes, it gives out hydrocarbon molecules. At very high temperature, these molecules dissociate to give hydrogen gas and carbon atoms that are deposited on the surface as char. This thin char layer was observed on all substrates. Some microcracks were observed on the a-LCA-p surface at post test.

(2) Partially Dense LCAs: Figure 7 shows mass loss flux plot for heating condition of $\dot{q}_{cw}$ = 830 Btu/ft^2-s and stagnation pressure of 0.081 atm. As shown in this figure, the partially dense LCAs suffered severe mechanical failure as early as 5 sec of exposure, especially the a-LCAs. One probable cause for this mechanical failure, sometimes referred to as spallation, is the rapid increase in surface temperature that results from the formation of a char layer on the model's surface. The increase in surface temperature, however, is not sufficient to initiate the vaporization of the ceramic fibers but is high enough to cause melting of the substrate. The model subsequently undergoes shape changes and the heating condition at the surface is further decreased, which accelerates the observed failure.

The AETB material was used as another substrate for the development of LCA's and is identified as a-LCAs. This substrate consists of a large quantity of alumina fibers that have higher melting temperature than that of silica fibers in the pure silica substrates. Thus, it can be expected that the bulk melting temperature of a-LCAs is higher than that of the s-LCAs.

The mass loss flux plots, however, show that the a-LCAs have higher recession rates compared to the s-LCAs. One of the reasons for this behavior is that the boron oxide in the aluminoborosilicate fibers in the AETB substrate became volatile at high temperature causing the SiO_2 fibers to devitrify, which lowers the bulk melting temperature of the AETB substrate (ref. 12). The high heating rate coupled with high stagnation pressure accelerates the structural failure within the fiber matrix. This plot also shows that the mass loss fluxes of the s-LCA-p's are comparable with the conventional ablators (SLA-561, Avcoat). Visual inspection at posttest indicated that the ablating surfaces of all LCAs consist of a char layer that is reinforced by a coalescent ceramic oxide melt layer, whereas the surfaces of SLA-561 and MA-25S consist of a powdery char and a thick brittle char layer respectively.

In order to prevent mechanical failure, the substrates used in LCA's development must be able to withstand high surface temperature (e.g., substrates have high melting points). Carbon Fiberform insulation and the AI-8 materials were added to the substrates test matrix (table 1) based on the above findings. Scanning electron microscopy (SEM) and TGA analysis of tested models also indicated that the distribution of resin within the fibrous matrix was not uniform for the partially dense LCAs. Better infiltration techniques were developed to obtain a uniform distribution of resins for Phases II and III.

b. 20 MW AHF Phase II Test– Three test conditions were used in Phase II to simulate various reentry peak heating environments for a Lunar return mission (ref. 13). The heat fluxes varied from 100 to 400 Btu/ft^2-sec, stagnation pressures from 0.018 to 0.062 atm, and the exposure time was 60 seconds.

Pre-test and post-test measurements are shown in table 4. Mass loss flux and recession data from high speed films for heat fluxes of 100, 200, and 400 Btu/ft^2-sec are plotted in figures 8, 9, and 10, respectively. One notable feature in these three figures is that the LI-900 baseline without resin and balsa wood have the highest mass loss fluxes or recession rates. It was observed that balsa wood and the LI-900 baseline undergo a significant shape change (increase in nose radius of curvature) with an associated reduction in convective heat flux. The LI-900 surface has a thick layer of coalescent melt, and the char layer on the balsa wood model is of a typical wood burned surface.

(1) Figure 8 showed that, at heat flux of ~100 Btu/ft^2-sec or below, the addition of SiC particles significantly reduced the recession rate and mass loss flux of the silica substrate—almost by 50%. The addition of high blowing (high rate of pyrolysis gas) resins such as pmma did not improve the materials' thermal performance due to a significant increase in the final density of the system. The effective mass loss fluxes of Avcoat, c-LCA-p, and s-LCA-p are comparable with the

AI-8 whereas the -sLCA-m, w-LCA, and balsa wood have the highest mass loss fluxes.

(2) At heat flux of 200 Btu/ft^2-sec, figure 9 shows that Acusil-1 and AI-8 have the lowest mass loss flux and balsa wood and s-LCAs have the highest. At this flux level, it is shown that the addition of pmma improved the performance of most LCA's substrates, especially the AI-8's, due to its high blowing characteristics of pmma. The decomposition and gas pyrolysis of pmma acts as a transpiration coolant to the silica surface and thus reduces the heating rate at the surface. This blowing characteristic of pmma combines with the high emittance characteristic of AI-8 significantly decreases the overall recession rates of AI-LCA-pm material.

The presence of phenolic in s-LCA-p, however, seems to cause a higher recession rate. Unlike pmma resin, the gas pyrolysis of phenolic resin has a much lower blowing rate and high char yield. Thus, the transpiration cooling effect from the gas pyrolysis process diminishes due to the low blowing characteristic, and a thick char layer is formed due to its high charring characteristics. The combination of these two effects caused the surface temperature to increase and subsequently the melting of the substrates.

(3) Figure 10 shows the stagnation point mass loss flux of LCAs at a heat flux of 400 Btu/ft^2-s and stagnation pressure of 0.061 atm. One interesting observation from these plots is that, at this flux level, the effects of non-charring and high blowing characteristics of pmma become less effective compared to the high charring and low blowing characteristics of phenolic. At this heating rate, it is believed that most energy at the surface is being rejected through a reradiation mechanism rather than through boundary layer blockage or transpiration cooling. However, the increase in surface temperature is still not sufficient to cause the vaporization of the substrate, but enough to trigger the melting of substrates.

The results in figure 10 also show that the c-LCAs are the most mass efficient system compared to all other LCAs and conventional ablators. It also showed that the mass loss flux of c-LCA-p is about half of that of the c-LCA-m and c-LCA because of the high charring characteristic of phenolic resin. The reason for the high mass efficiency of c-LCA-p is twofold. First, for the LCAs with phenolic infiltrant, most energy at the surface is being rejected by reradiation mechanism due to the thick char layer formed by the decomposition of phenolic. Second, the c-LCA-p's have a carbon substrate that has very high melting temperature (>5,000°F in inert environment or vacuum) compared to that of the silica substrates. The substrate remains stable even with an increase in surface temperature. Thus, most of the absorbed energy at the c-LCA-ph's surface is reradiated by both carbon substrate (emittance = 0.9) and the char layer.

As mentioned in the material section, two of each s-LCA-p and s-LCA-m were instrumented with thermocouple stack to obtain the thermal response of these two systems.

Figures 11 and 12 show the surface and in-depth temperature plots of selected LCAs at heat flux 100 and 200 Btu/ft^2-sec, respectively. The surface temperature profiles shown in these figures are obtained from an optical pyrometer (emittance was set at 1.0 on the pyrometer) and are corrected by using total hemispherical emittance of 0.5 for all s-LCAs. Other profiles are the in-depth temperatures obtained from the thermocouples. Two general observations can be made from these plots. First, the surface and backface temperatures at heat flux levels of 100 and 200 Btu/ft^2-sec are similar. Second, the in-depth temperature profiles of LCAs with phenolic infiltrant are slightly higher than that of LCAs with pmma infiltrant. This behavior is expected because the phenolic resin has higher thermal conductivity than that of pmma and that the internal gas percolation and decomposition products of phenolic also have higher thermal conductivity.

Figures 13(a) and 13(b) show the surface temperatures obtained from an optical pyrometer for all tested samples including the Avcoat and Acusil-1. The surface temperatures are corrected by using the total hemispherical emittance of 0.90 for the c-LCAs and 0.50 for the s-LCAs. The surface temperature of c-LCAs peaked at 4300°F whereas Acusil-1 peaked at 2,500°F and is shown in figure 13(a). It is observed that the surface temperature is affected either by the blowing or the charring characteristics of the resins. This is evident by the ~200°F difference in surface temperatures between the s-LCA-m (~3400°F) and the s-LCA-p (~3600°F) as shown in figure 13(b).

c. 60 MW IHF Phase III Test– A similar material test matrix was used in the 60MW IHF Phase III, but with the addition of the c/oak-LCA (CBCF insulation from Oakridge National Laboratory). The objective of this test series was to evaluate the thermal performance of LCAs at high heat fluxes (simulated Mars returned mission trajectory) of 830 and 1,440 Btu/ft^2-sec and stagnation pressures of 0.081 and 0.333 atm. Pre-test and post-test measurements are reported in table 5.

The stagnation point recession data of all the tested samples as a function of time are shown in figure 14 for a heat flux of 830 Btu/ft^2-s and stagnation pressure of

0.081 atm. One notable feature in this plot is the high recession rate of the balsa wood (sample survived less than 5 sec of exposure) and the low recession rates of c-LCA-p's. This figure also showed that all c-LCAs generally have better performance than the s-LCAs including the SLA-561 and MA-25S.

The superior performance of c-LCA's is further evident by the mass loss flux shown in figure 15. This figure showed that the c-LCA-p has the lowest mass loss flux and balsa wood has the highest. This plot also showed that the addition of pmma (high blowing resin) did not improve the performance of c-LCAs but also decreased the mass efficiency of this system. The c-LCA-oak material has a slightly higher recession rate compared to the c-LCA and c-LCA-p. This result coupled with visual observation indicated that the addition of phenolic particles is not as efficient as the impregnation of phenolic into the carbon substrate as reported in the materials section. Visual observation indicated that no spallation or only microspallation took place during the testing of the c-LCAs. The LI-2200, which has 1.5% by weight of SiC, exhibits similar ablation characteristic as the phenolic impregnated s-LCAs and the conventional ablators (Avcoat and MA-25S). Figure 15 also shows that the s-LCA-m and SLA-561 have identical mass loss flux. The s-LCA-w and balsa wood appeared to be the least efficient systems. It was observed that Avcoat, SLA-561, and s-LCAs undergo a significant shape change, and severe spallation during test.

In general, the preliminary test results indicate that at high flux levels, the reradiation mechanism is a main heat dissipation process, and the boundary layer blockage due to polymer decomposition became a secondary mechanism.

Four of the best performing materials were selected for testing at heating rate of 1,440 Btu/ft^2-sec. As shown in figure 16, the LI-2200 suffered severe mechanical failure at 10 sec while the c-LCA-p survived a full 30 sec exposure. However, from visual inspection of high speed films, it was determined that spallation occurred at 20 sec during the testing of the un-infiltrated c-LCAs. Surface erosion and spallation were also observed after 20 sec during the test of the c-LCA-oak sample. No similar behavior was detected for c-LCA-p, there could be spallation in the microstage that is not detectable. Figure 16 shows that both c-LCA-p and c-LCA-oak have similar mass loss fluxes, but upon post-test inspection, the c-LCA-oak suffered some surface erosion.

Finally, the effective heat of ablation is a quantity often used to determine the materials efficiency at a given heating rate. Figure 17 shows the mass efficiency of materials used in three arc-jet tests as a function of cold wall heat fluxes. Several important observations can be made from this plot. Because of the high melting temperature and high emittance of the carbon substrates, the c-LCA-p's have the highest effective heat of ablation at heat fluxes above 400 Btu/ft^2-sec. Below this flux level, the kinetic mechanism (i.e., oxidation of carbon) is more favorable, making the c-LCAs less efficient. At low flux levels of ~100 Btu/ft^2-s and low pressure (0.018 atm), the AI-8 and Acusil-1 are more mass efficient than all the LCAs as well as the Avcoat and SLA-561. At 200 Btu/ft^2-s, AI-8-m's are more mass efficient due to the high blowing characteristics of the pmma infiltrant. Overall, balsa wood and s-LCA-w's are the least efficient systems, and SLA-561 and Avcoat maintain average performance at all heat flux levels.

Conclusion

A series of lightweight ceramic ablators were developed and tested to evaluate their thermal performance with the traditional ablators such as SLA-561, MA-25S, and Avcoat-5026. It was shown that the c-LCAs with either no infiltrant or with phenolic infiltrant are the most mass efficient systems at heat fluxes above 400 Btu/ft^2-s. No spallation, no mechanical failure, and no shape changes were observed during the testing of these c-LCAs up to heat flux of 1100 Btu/ft^2-s.

The addition of SiC improved the thermal performance of silica substrates (AI-8's) due to a significant increase in the total hemispherical emittance of the substrates. The presence of pmma in AI-8s showed little effect at a flux level of ~100 Btu/ft^2-s but greatly improved the AI-LCA's performance at flux level of 200 Btu/ft^2-s. For the case of s-LCA-m test samples, spallation and mechanical failure became more severe at flux levels above 100 Btu/ft^2-s. The traditional ablators such as Avcoat, SLA-561, and Acusil-1 maintain average performance at low flux levels except for Acusil-1, which, at 100 Btu/ft^2-s, has the highest effective heat of ablation, H_{eff}. The general performance of s-LCA-p's is very similar to the conventional ablators; but significant melt runoff was observed at the high flux levels. Balsa wood and s-LCA-w's undergo a shape change along with spallation that results in high recession rates and a low effective heat of ablation.

References

1. Henline, W. D.: Aerothermodynamic Heating Environment and Thermal Protection Materials Comparison for Manned Mars–Earth Return Vehicles. AIAA Paper 91-0697, 29th Aerospace Science Meeting, Reno, Nev., Jan. 7–10, 1991.
2. Lane, J.: An Evaluation of Ablative Materials for an LTV Aerobrake. Phase II Study Final Report – Aerobrake Assembly With Minimum Accommodation, MDSSC IRAD PD 01-286, Jan. 23, 1992.
3. For Materials Ingenuity, Some Comments on the Thermal Conductivity of Carbon Fiberform Insulation. FMI – Fiber Materials, Inc. internal report.
4. Wei, G. C.; and Robins, J. M.: Carbon-Bonded Carbon Fiber Insulation for Radioisotope Space Power Systems. American Society Bulletin, vol. 64, no. 5, May 1985.
5. Bartlett, E. P.; and Andersen, L. W.: An Evaluation of Ablation Mechanism for the Apollo Heat Shield Material. Aerotherm Report No. 68-38, Part II, Oct. 15, 1968.
6. Williams, S. D.: Thermophysical Properties used for Ablation Analysis. LEC-13999, Dec. 1979.
7. Beck, R. A. S.; and Blaub, B.: Materials Development for Multiple Performance Requirements. SAE 840920, July 16–19, 1984.
8. Balter–Peterson, A.; Nichols, F.; Mifsud, B.; and Love, W.: Arc Jet Testing in NASA Ames Research Center Thermophysics Facilities. AIAA Paper 92-5041, AIAA Fourth International Aerospace Planes Conference, Dec. 1–4, 1992.
9. Stewart, D. A.; and Kolodziej, P.: Heating Distribution Comparison Between Asymmetric Blunt Cones. AIAA Paper 86-1307, June 1986.
10. Henline, W. D.; Tran, H. K.; and Hamm, M. K.: Phenomenological and Experimental Study of the Thermal Response of Low Density Silica Ablators to High Enthalpy Plasma Flow. AIAA Paper 91-1324, 26th Thermophysics Conference, June 24–26, 1991.
11. Milos, F. S.; and Rasky, D. J.: A Review of Numerical Procedures for Computational Surface Thermochemistry. AIAA Paper 92-2944, 1992.
12. Stewart, D. A.; and Leiser, D. B.: Thermal Stability of Ceramic Coated Thermal Protection Materials in a Simulated High-Speed Earth Entry. Ceramic Eng. Sci. Proc., 9[9–10], 1988, pp. 1199–1206.
13. Russell, J. W.: Lunar Aerobrake Thermal Protection System Analysis. Phase II Study Final Report – Aerobrake Assembly with Minimum Accommodation, Jan. 23, 1992.

Table 1a. LCA material test matrix

LCA identification	Substrate composition, % by wt.	Substrate density, lbm/ft^3	Infiltrant	LCA density, lbm/ft^3
AI-8	98.5% SiO_2 1.5% SiC particles	7.9–8.8	none	7.9–8.8
AI-8m	98.5% SiO_2 1.5% SiC particles	7.9–8.8	pmma	13.4–14.5
s-LCA-m	LI-900 100% SiO_2	8.8–9.3	pmma	13.3–14.8
s-LCA-e	LI-900 100% SiO_2	8.8–9.3	epoxy	13.3–14.8
s-LCA-p	LI-900 100% SiO_2	8.8–9.3	phenolic	13.3–14.8
a2-LCA-m a2-LCA-e a2-LCA-p	AETB-20-8 70.88% SiO_2 27.44% Al_2O_3 1.68% B_2O_3	7.9–8.3	pmma epoxy phenolic	13.3–14.8
a5-LCA-m a5-LCA-e a5-LCA-p	AETB-50-8 38% SiO_2 57.44% Al_2O_3 1.68% B_2O_3	7.8–8.3	pmma epoxy phenolic	13.3–14.8
c-LCA-m	FMI carbon 100% carbon	10.8–11.3	pmma	14–15.5
c-LCA-p	FMI carbon 100% carbon	10.8–11.3	phenolic	14–15.5
c-LCA-oak	Oakridge CBCF with phenolic particles	17	none	17

Table 1b. Conventional ablators test matrix

Model I.D.	Composition	Density, lbm/ft^3	Test condition heat flux, Btu/ft^2-s
Avcoat-5026-39HC	Phenolic microballoons Novalac Resin Phenolic honeycomb cells	32.00	100 200 400 830
MA-25S (MM)	Filled Elastomeric silicone	25.31	100 200 400 830
SLA-561 (MM)	Elastomeric silicone Silica fibers Carbon black Cork Microballoons	17.1	830 1150
ACUSIL-1 (Acurex)	Silicone resin Flexcore glass phenolic H/C Quartz & phenolic microballoons Quartz fibers	30.10	100 200 400

Table 2a. Lightweight ceramic ablators nominal test conditions

$\dot{q}$, Btu/ft^2-s	Stag. pressure, atm	Enthalpy, Btu/lbm	Model radius, in.
100	0.014	5.851E+03	1.00
200	0.0256	8.653E+03	1.00
400	0.0609	1.122E+04	1.00
600	0.0766	1.061E+04	0.50
830	0.081	1.428E+04	0.50
1120	0.141	1.460E+04	0.50
1400	0.330	1.193E+04	0.50

Table 2b. GCMS analysis of polymeric infiltrants

Infiltrants	Carbon, %	Oxygen, %	Hydrogen, %
PMMA	24.20	N/D*	0.33
Epoxy	78.66	N/D	0.77
Phenolic	96.43	1.77	0.92

*N/D: Unable to detect.

Table 3. 60 MW Phase I – pre- and post-test measurements

60 MW IHF 50 -LIGHT WEIGHT ABLATORS TEST															
Model I.D.	Substrate	Filler	Density (lbm/cuft)	Test time (sec)	Pyro. readings (MS 5816 (K)	(F)	Initial Length (in)	Final Length (in)	Recession (in)	S dot (in/sec) ΔA/ΔT	sdot ft/sec	Initial Wt. (gm)	Final Wt. (gm)	Mass Loss (gm)	Heff (BTU/lbm) based on sdot
Q DOT(CW) = 830 BTU/FT2-SEC AND PT2= 0.081ATM															
L9F11-PM	LI-900	PMMA	62.60	25	2400	3860	3.497	3.289	0.208	8.320E-03	6.933E-04	42.98	36.05	6.93	1.912E+04
L9F31-EP	LI-900	EPOXY	79.95	30	2500	4040	3.514	3.225	0.289	9.633E-03	8.028E-04	55.17	48.95	6.22	1.293E+04
L9F51-PH	LI-900	PHENOLIC	71.88	30	2500	4040	3.571	3.45	0.121	4.033E-03	3.361E-04	50.45	43.71	6.74	3.435E+04
A5F71-PM	AETB-8-50	PMMA	66.51	30	2700	4400	3.487	3.247	0.24	8.000E-03	6.667E-04	45.53	37.63	7.9	1.872E+04
A5F91-EP	AETB-8-50	EPOXY	81.24	30	2500	4040	3.505	3.42	0.085	2.833E-03	2.361E-04	55.91	48.69	7.22	4.327E+04
A5F111-PH	AETB-8-50	PHENOLIC	69.52	30	2750	4490	3.398	3.245	0.153	5.100E-03	4.250E-04	46.31	39.64	6.67	2.809E+04
L9P131-PM	LI-900	PMMA	14.14	20	2100	3320	3.491	2.36	1.131	5.655E-02	4.713E-03	9.69	6.13	3.56	1.246E+04
L9P161-EP	LI-900	EPOXY	13.77	25	2200	3500	3.495	2.125	1.37	5.480E-02	4.567E-03	9.45	5.38	4.07	1.320E+04
L9P191-PH	LI-900	PHENOLIC	13.77	30	2300	3680	3.5	2.328	1.172	3.907E-02	3.256E-03	9.46	6.07	3.39	1.852E+04
A2P221-PM	AETB-8-20	PMMA	13.13	10	2100	3320	3.495	1.75	1.745	1.745E-01	1.454E-02	9.01	4.35	4.66	4.347E+03
A2P251-EP	AETB-8-20	EPOXY	13.84	20	2300	3680	3.495	1.665	1.83	9.150E-02	7.625E-03	9.5	4.34	5.16	7.862E+03
A2P281-PH	AETB-8-20	PHENOLIC	13.75	20	2500	4040	3.49	1.836	1.654	8.270E-02	6.892E-03	9.42	4.5	4.92	8.760E+03
A5P311-PM	AETB-8-50	PMMA	13.42	10	2000	3140	3.485	1.8	1.685	1.685E-01	1.404E-02	9.18	4.5	4.68	4.405E+03
A5P341-EP	AETB-8-50	EPOXY	13.48	15	2300	3680	3.495	1.75	1.745	1.163E-01	9.694E-03	9.25	4.22	5.03	6.351E+03
A5P381-PH	AETB-8-50	PHENOLIC	13.37	25	2500	4040	3.505	1.725	1.78	7.120E-02	5.933E-03	9.2	4.05	5.15	1.046E+04
SLA-561-41	SLA-561	VARIOUS	17.09	30	2350	3770	3.55	2.455	1.095	3.650E-02	3.042E-03	11.92	7.6	4.32	1.597E+04
AVCO-43	H/C	PHENOLIC	34.38	30	2300	3680	3.247	2.8	0.447	1.490E-02	1.242E-03	21.83	16.3	5.53	1.945E+04
MA-25S53-1	RUBBER	MM	28.42	30	2300	3680	3.51	2.886	0.624	2.080E-02	1.733E-03	19.59	15.27	4.32	1.685E+04
L945-1	LI-900	NONE	8.25	10	ND	ND	3.5	1.22	2.28	2.280E-01	1.900E-02	5.67	2.76	2.91	5.295E+03
A247-1	AETB-8-20	NONE	7.88	8	2300	3680	3.484	1.325	2.159	2.699E-01	2.249E-02	5.39	2.11	3.28	4.683E+03
A549-1	AETB-8-50	NONE	7.99	5	2400	3860	3.495	1.41	2.085	4.170E-01	3.475E-02	5.48	2.19	3.29	2.991E+03
LI2203	LI-2200	NONE	22.00	30	2160	3428			0.423	1.410E-02	1.175E-03	112.01	110.9	1.11	3.211E+04
Q DOT(CW) = 1100 BTU/FT2-SEC AND PT2= 0.141											0.000E+00				
SLA-561-42	SLA-561	VARIOUS	17.79	30	2350	3770	3.545	1.87	1.675	5.583E-02	4.653E-03	12.39	5.7	6.69	1.003E+04
AVCO-44	H/C	PHENOLIC	33.92	30	2700	4400	3.255	2.735	0.52	1.733E-02	1.444E-03	21.6	14.77	6.83	1.694E+04
MA-25S54			28.32	30	2300	3680	3.51	2.6	0.91	3.033E-02	2.528E-03	19.52	13.54	5.98	1.159E+04
L9F22-PM	LI-900	PMMA	62.45	30	2700	4400	3.505	3.12	0.385	1.283E-02	1.069E-03	42.98	34.07	8.91	1.243E+04
L9F42-EP	LI-900	EPOXY	80.02	30	2900	4760	3.48	2.65	0.83	2.767E-02	2.306E-03	54.66	39.41	15.25	4.499E+03
L9F62-PH	LI-900	PHENOLIC	69.12	30	3000	4940	3.57	3.395	0.175	5.833E-03	4.861E-04	48.5	40.08	8.42	2.470E+04
A5F82-PM	AETB-8-50	PMMA	65.30	25	2700	4400	3.475	3.325	0.15	6.000E-03	5.000E-04	44.54	39.17	5.37	2.542E+04
A5F122-PH	AETB-8-50	PHENOLIC	64.53	30	3000	4940	3.505	3.1	0.405	1.350E-02	1.125E-03	44.41	36.26	8.15	1.143E+04
L9P142-PM	LI-900	PMMA	13.23	15	2200	3500	3.495	2.295	1.2	8.000E-02	6.667E-03	9.08	6	3.08	9.409E+03
L9P202-PH	LI-900	PHENOLIC	14.25	20	2450	3950	3.498	2.2	1.298	6.490E-02	5.408E-03	9.79	5.99	3.8	1.077E+04
A2P232-PM	AETB-8-20	PMMA	13.42	7	2100	3320	3.496	1.555	1.941	2.773E-01	2.311E-02	9.21	4.62	4.59	2.677E+03
A2P292-PH	AETB-8-20	PHENOLIC	13.75	18	2600	4220	3.485	1.8155	1.6695	9.275E-02	7.729E-03	9.41	4.96	4.45	7.807E+03
A5P322-PM	AETB-8-50	PMMA	13.36	5	1900	2960	3.485	1.84	1.645	3.290E-01	2.742E-02	9.14	4.79	4.35	2.266E+03
A5P392-PH	AETB-8-50	PHENOLIC	13.37	15	2900	4760	3.505	2.825	0.68	4.533E-02	3.778E-03	9.2	6.25	2.95	1.644E+04
LI2204	LI-2200	NONE	22	30	2200	3500			0.66	2.200E-02	1.833E-03	127.38	125.64	2.95	2.058E+04

Table 4. 20 MW Phase II – pre- and post-test measurements

SCA-20MW ARC JET TEST MATRIX															
MODEL ID	SUBSTRATE	FILLER	Run no.	Time, sec	Initial wt. gm	final wt., gm	wt. loss, gm	mdot, lbm/se	initial L, in	final L, in.	delta L, in	adot, ft/sec	Density	heat flux,	heff,edot
													lb/ft3	Btu/ft2-s	Btu/lbm
L2900	LI900		14	60	30.17	30.08	0.09	3.308E-06	4.48	3.9	0.58	8.056E-04	8.81	1.000E+02	1.408E+04
L2911-PM	LI900	PMMA	11	120	51.17	40.62	10.55	1.939E-04	4.504	4.091	0.413	2.868E-04	14.86	1.000E+02	2.346E+04
L2922-PM	LI900	PMMA	12	120	46.48	33.23	13.25	2.435E-04	4.49	3.362	1.128	7.833E-04	13.55	2.000E+02	1.885E+04
L2933-PM	LI900	PMMA	26	42	46.15	35.7	10.45	5.486E-04	4.478	3.515	0.963	1.911E-03	13.49	4.000E+02	1.552E+04
L2944-PM	LI900	PMMA	46	60	48.143	39.03	9.113	3.349E-04	4.492	3.982	0.51	7.083E-04	14.02	2.000E+02	2.013E+04
L2955-PM	LI900	PMMA	47	60	47.344	40.8	6.544	2.405E-04	4.49	4.289	0.201	2.792E-04	13.80	1.000E+02	2.596E+04
L2961-PH	LI900	PHENOLIC	25	60	48.5	35.91	12.59	4.627E-04	4.476	4.37	0.106	1.472E-04	14.18	1.000E+02	4.789E+04
L2972-PH	LI900	PHENOLIC	24	60	47.605	42.7	4.905	1.803E-04	4.464	4.091	0.373	5.181E-04	13.96	2.000E+02	2.765E+04
L2983-PH	LI900	PHENOLIC	29	60	48.21	36.74	11.47	4.215E-04	4.498	3.565	0.933	1.296E-03	14.02	4.000E+02	2.201E+04
L2994-PH	LI900	PHENOLIC	43	120	48.42	38.52	9.9	1.819E-04	4.492	3.845	0.647	4.493E-04	14.11	1.000E+02	1.578E+04
L29105-PH	LI900	PHENOLIC	44	120	48.15	40.64	7.51	1.380E-04	4.524	4.355	0.169	1.174E-04	13.92	2.000E+02	1.224E+05
L29S00	LI900		17	60	28.46	28.43	0.03	1.103E-06	4.484	4.3	0.184	2.556E-04	8.31	1.000E+02	4.711E+04
L29S111-PM	LI900	PMMA	16	60	51.08	47.14	3.94	1.448E-04	4.484	4.388	0.096	1.333E-04	14.91	1.000E+02	5.031E+04
L29S122-PM	LI900	PMMA	19	60	51.5	46.16	5.34	1.963E-04	4.547	4.32	0.227	3.153E-04	14.81	2.000E+02	4.284E+04
L29S133-PM	LI900	PMMA	27	40	49.49	40.4	9.09	5.011E-04	4.512	3.735	0.777	1.619E-03	14.35	4.000E+02	1.722E+04
L29S144-PM	LI900	PMMA	48	120	47.164	41.1	6.064	1.114E-04	4.5	4.322	0.178	1.236E-04	13.71	1.000E+02	5.899E+04
CF161-PH	CARBON	PHENOLIC	38	60	59.751	54.76	4.991	1.834E-04	4.504	4.4	0.104	1.444E-04	17.36	1.000E+02	3.989E+04
CF181-PM	CARBON FIBER	PMMA	35	60	59.32	45.28	14.04	5.160E-04	4.501	4.061	0.44	6.111E-04	17.24	4.000E+02	3.796E+04
CF46	CARBON	NONE	37	60	41.08	36.05	5.03	1.849E-04	4.47	3.985	0.485	6.736E-04	12.03	4.000E+02	4.936E+04
CF174-PH	CARBON	PHENOLIC	36	60	58.45	49.56	8.89	3.267E-04	4.484	4.162	0.322	4.472E-04	17.06	4.000E+02	5.243E+04
BW22	BALSA WOOD	NONE	13	70	35.52	19.39	16.13	5.081E-04	4.547	2.878	1.669	1.987E-03	10.21	2.000E+02	9.857E+03
BW23	BALSA WOOD	NONE	30	40	31.37	19.87	11.5	6.340E-04	4.559	2.845	1.714	3.571E-03	8.99	4.000E+02	1.246E+04
BW25	BALSA WOOD	NONE	10	60	32.104	21.98	10.124	3.721E-04	4.539	3.618	0.921	1.279E-03	9.25	1.000E+02	8.453E+03
AVCOAT-27	CORK	MICROBALOON	39	60	71.13	62.41	8.72	3.205E-04	4.54	4.476	0.064	8.889E-05	32.00	1.000E+02	3.516E+04
AVCOAT-28	CORK	MICROBALOON	40	60	69.49	57.63	11.86	4.359E-04	4.54	4.31	0.23	3.194E-04	32.00	2.000E+02	1.957E+04
AVCOAT-29	CORK	MICROBALOON	31	60	70.21	53.75	16.46	6.049E-04	4.53	4.13	0.4	5.556E-04	32.00	4.000E+02	2.250E+04
AVCOAT-30	CORK	MICROBALOON	49	120	71.17	57.29	13.88	2.551E-04	4.563	4.382	0.181	1.257E-04	20.38	1.000E+02	3.903E+04
MA25S-32	MARTIN MARRIETTA		15	75	101.63	97.56	4.07	1.197E-04	4.522	4.642	-0.12	-1.333E-04	29.39	1.000E+02	-2.552E+04
MA25S-33	MARTIN MARRIETTA		20	60	99.63	94.45	5.18	1.904E-04	4.545	4.422	0.123	1.708E-04	28.66	2.000E+02	4.085E+04
MA25S-34	MARTIN MARRIETTA		32	60	103.85	89.72	14.13	5.193E-04	4.54	3.92	0.62	8.611E-04	29.91	4.000E+02	1.553E+04
MA25S-35	MARTIN MARRIETTA		45	60	101.86	96.21	5.65	2.076E-04	4.53	4.431	0.099	1.375E-04	29.40		0.000E+00
ACUSIL-39	ACUREX		22	60	261.05?	258.41	2.8	1.029E-04	4.53	4.5	0.03	4.167E-05	30.00	1.000E+02	8.000E+04
ACUSIL-40	ACUREX		23	60	255.98	250.76	3.1	1.139E-04	4.54	4.485	0.01	1.389E-05	30.00	2.000E+02	4.800E+05
ACUSIL-41	ACUREX		34	40	230.8	214.97	11.61	6.400E-04	4.515	4.2	0.323	6.729E-04	30.00	4.000E+02	1.981E+04
L2942-W	LI-900	WATER	18	60	205.51	150.25	55.26	2.031E-03	4.215	4.19	0.025	3.472E-05	64.14	1.000E+02	4.490E+04
L2943-W	LI-900	WATER	21	60	207.74	152.7	55.04	2.023E-03	4.238	4.23	0.008	1.111E-05	64.45	2.000E+02	2.793E+05
L2944-W	LI-900	WATER	28	60	205.88	140.74	65.14	2.394E-03	4.238	3.855	0.383	5.319E-04	63.88	4.000E+02	1.177E+04

Table 5. 60 MW Phase III – pre- and post-test measurements

60 MW IHF TEST RESULTS PHASE III - LIGHT WEIGHT CERAMIC ABLATORS																	
	SUBSTRATE	FILLER	LENGTH (cm)	LENGTH Inches	Initial mass gm	DENSITY (lb/ft3)	Run No.	Qdot Btu/ft2-s	time sec	Final Wt,gm	final L, in.	mass loss,gm	delta S,in	S dot ft/sec	post test density blm/ft3	Heffect,edot Btu/blm
FMI301-PM	CARBON	PMMA	10.06	3.96	11.76	14.82	3	830.00	30.00	7.750	3.531	4.010	0.430	1.193E-03	10.637	6.538E+04
FMI302-PM	CARBON	PMMA	10.21	4.02	12.25	15.93	22	830.00	60.00	6.170	3.235	6.080	0.785	1.090E-03	9.243	8.239E+04
FMI303-PM	CARBON	PMMA	10.22	4.02	12.27	15.82	30	830.00	60.00	6.070	3.207	6.200	0.817	1.134E-03	9.173	7.978E+04
FMI305-PH	CARBON	PHENOLIC	10.17	4.00	12.62	15.66	6	830.00	30.00	9.940	3.770	2.680	0.234	6.498E-04	12.778	9.996E+04
FMI306-PH	CARBON	PHENOLIC	10.21	4.02	12.55	15.40	21	830.00	60.00	8.140	3.532	4.410	0.488	6.773E-04	11.169	1.903E+05
FMI307-PH	CARBON	PHENOLIC	10.12	3.98	12.15	15.29	16	1440.00	30.00	8.040	3.338	4.110	0.646	1.795E-03	11.673	3.961E+04
FMI308-PH	CARBON	PHENOLIC	10.25	4.04	11.67	15.44	28	830.00	60.00	7.770	3.486	3.900	0.549	7.631E-04	10.802	1.007E+05
LI309-PM	LI900	PMMA	10.11	3.98	11.09	14.33	4	830.00	30.00	6.540	2.405	4.550	1.575	4.376E-03	13.179	1.439E+04
LI313-PH	LI900	PHENOLIC	10.20	4.02	11.41	14.88	8	830.00	30.00	8.120	3.111	3.290	0.905	2.513E-03	12.649	2.611E+04
OR317G	CARBON FELT	PHEN PART	9.84	3.87	7.39	17.11	26	830.00	30.00	5.300	3.535	2.090	0.339	9.417E-04	7.266	1.213E+05
OR318G	CARBON FELT	PHEN PART	10.09	3.97	7.64	17.21	27	1440.00	30.00	5.410	3.320	2.230	0.652	1.812E-03	7.897	1.006E+05
OR319G	CARBON FELT	PHEN PART	10.08	3.97	7.66	17.32	31	830.00	60.00	4.900	3.318	2.760	0.651	9.035E-04	7.157	1.284E+05
LIW328	LI900	WATER	10.20	4.02	6.48	8.03	9	830.00	30.00	5.770	3.470	0.710	0.546	1.516E-03	8.059	6.794E+04
BW321	Balsa Wood	NONE	10.34	4.07	7.57	9.62	5	830.00	5.00	3.080	2.452	4.490	1.619	2.698E-02	6.088	5.053E+03
AV324		NONE	8.24	3.24	21.32	33.32	10	830.00	30.00	16.540	2.865	4.780	0.379	1.053E-03	27.978	2.817E+04
AV325		NONE	8.20	3.23	21.46	34.49	11	1440.00	30.00	12.370	1.750	9.090	1.478	4.107E-03	34.256	1.024E+04
AV326		NONE	8.28	3.26	21.87	34.79	19	830.00	60.00	14.010	2.475	7.860	0.785	1.090E-03	27.433	2.776E+04
FMI332	CARBON	NONE	10.14	3.99	7.62	9.98	29	830.00	60.00	5.370	3.127	2.250	0.865	1.202E-03	8.323	8.300E+04
FMI333	CARBON	NONE	10.22	4.02	7.74	10.27	20	830.00	60.00	5.580	3.241	2.160	0.783	1.087E-03	8.344	9.152E+04
FMI334	CARBON	NONE	10.20	4.02	7.66	10.11	14	1440.00	30.00	3.840	2.189	3.820	1.827	5.074E-03	8.502	3.338E+04
FMI335	CARBON	NONE	10.13	3.99	7.69	10.29	2	830.00	30.00	6.470	3.558	1.220	0.430	1.195E-03	8.813	7.882E+04
LI336	LI900	H RESIN	10.15	4.00	11.05	14.31	7	830.00	30.00	7.990	3.098	3.060	0.898	2.495E-03	12.499	2.662E+04
SLA561-341		NONE	8.95	3.52	12.00	17.46	25	830.00	30.00	6.020	2.032	5.980	1.492	4.143E-03	14.358	1.395E+04

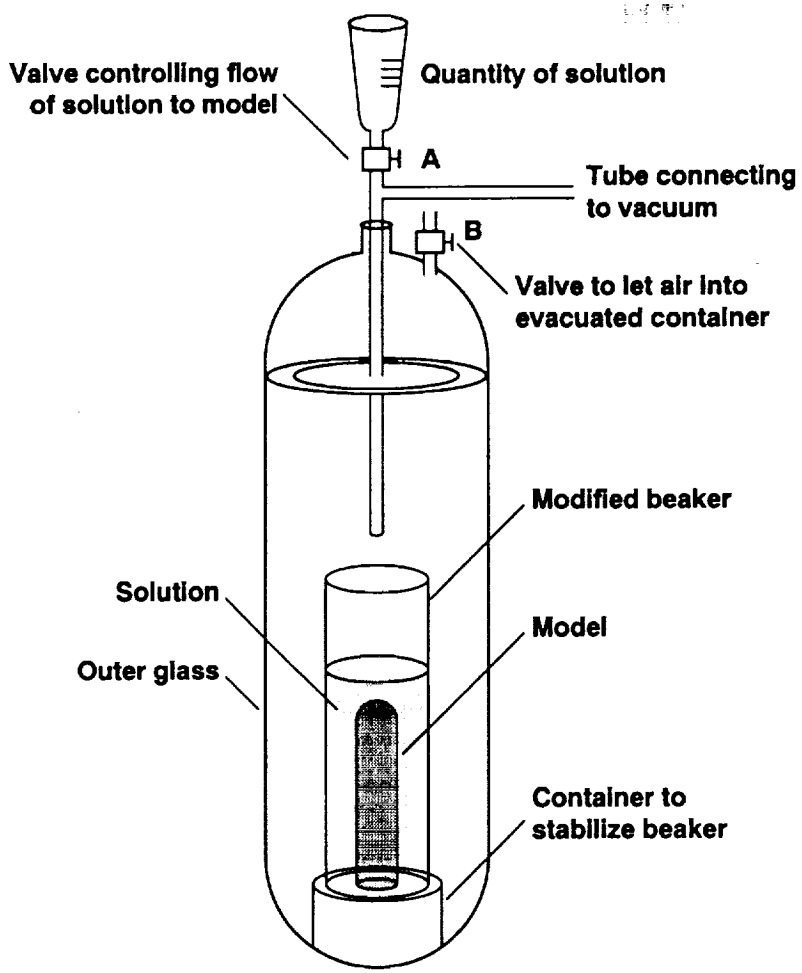

Figure 1. Infiltration apparatus for LCA models.

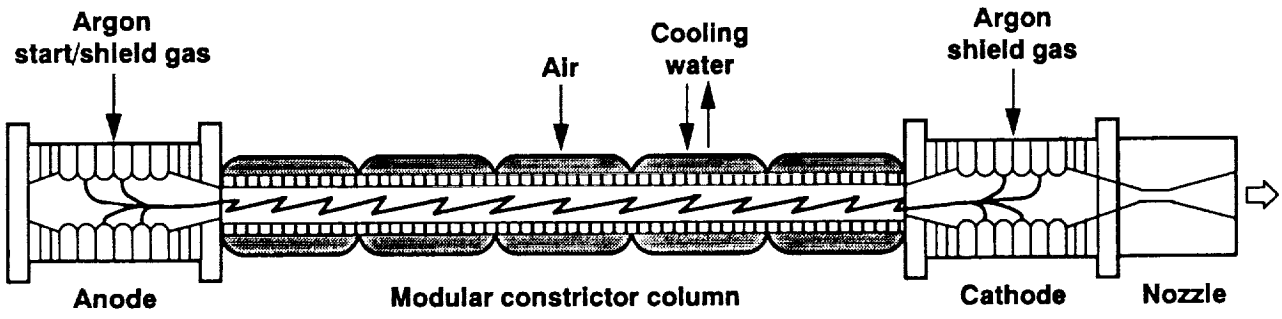

Figure 2. Illustration of segmented arc heater features.

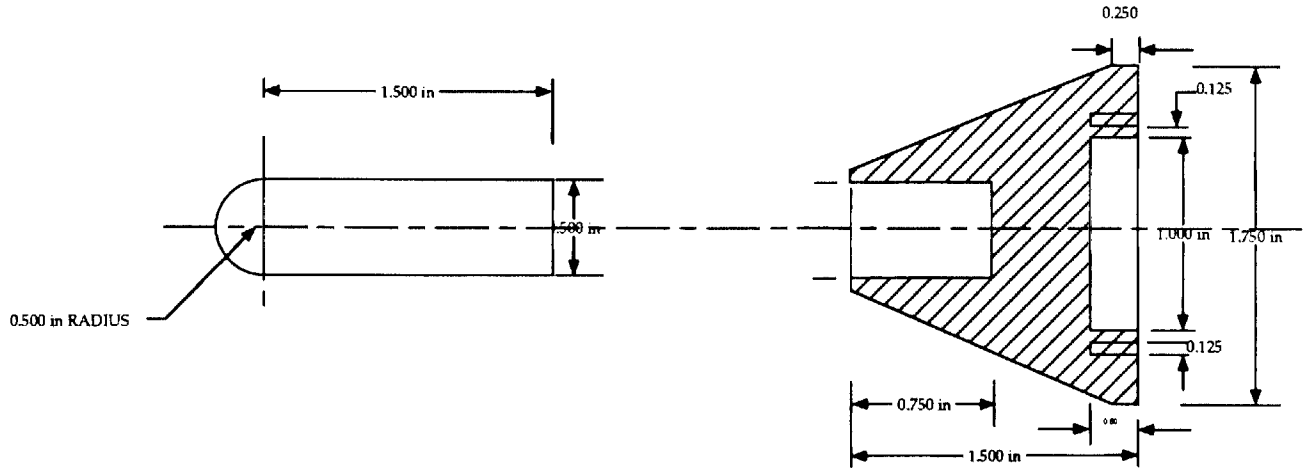

60 MW PHASE I & III - LCA TEST MODEL

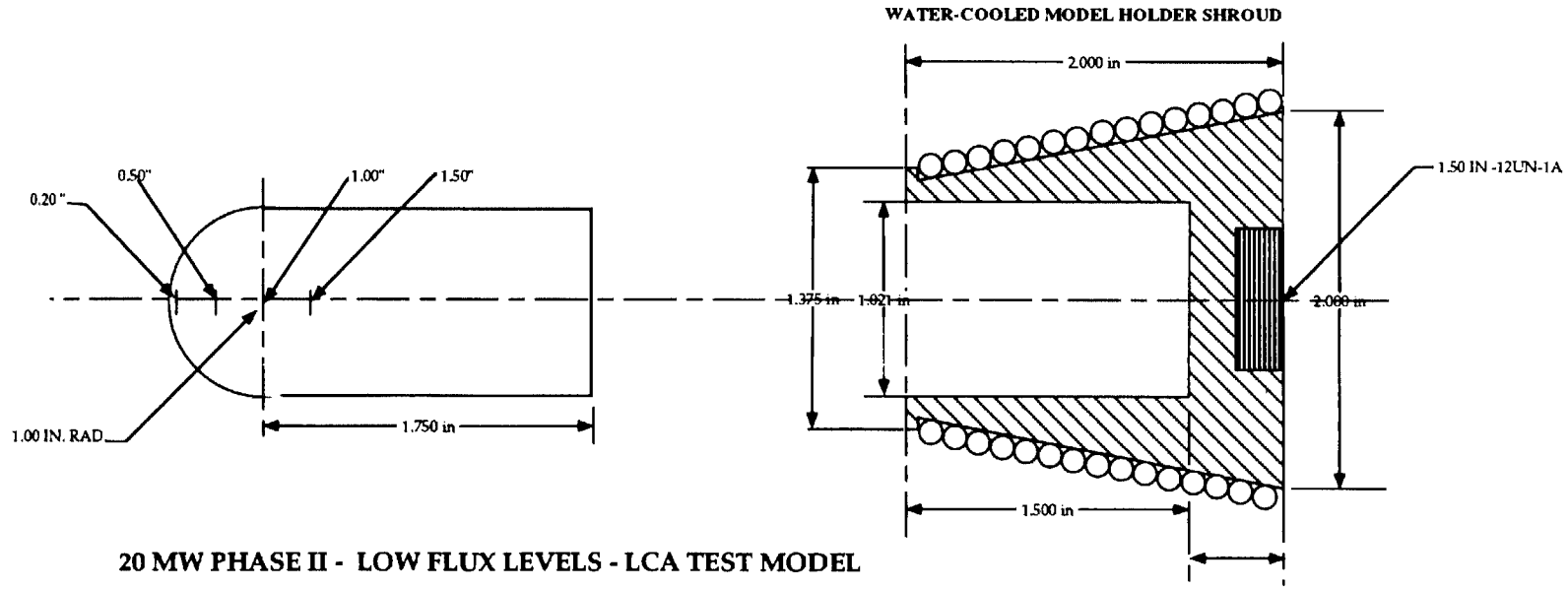

20 MW PHASE II - LOW FLUX LEVELS - LCA TEST MODEL

Figure 3. Arc-jet test model designs.

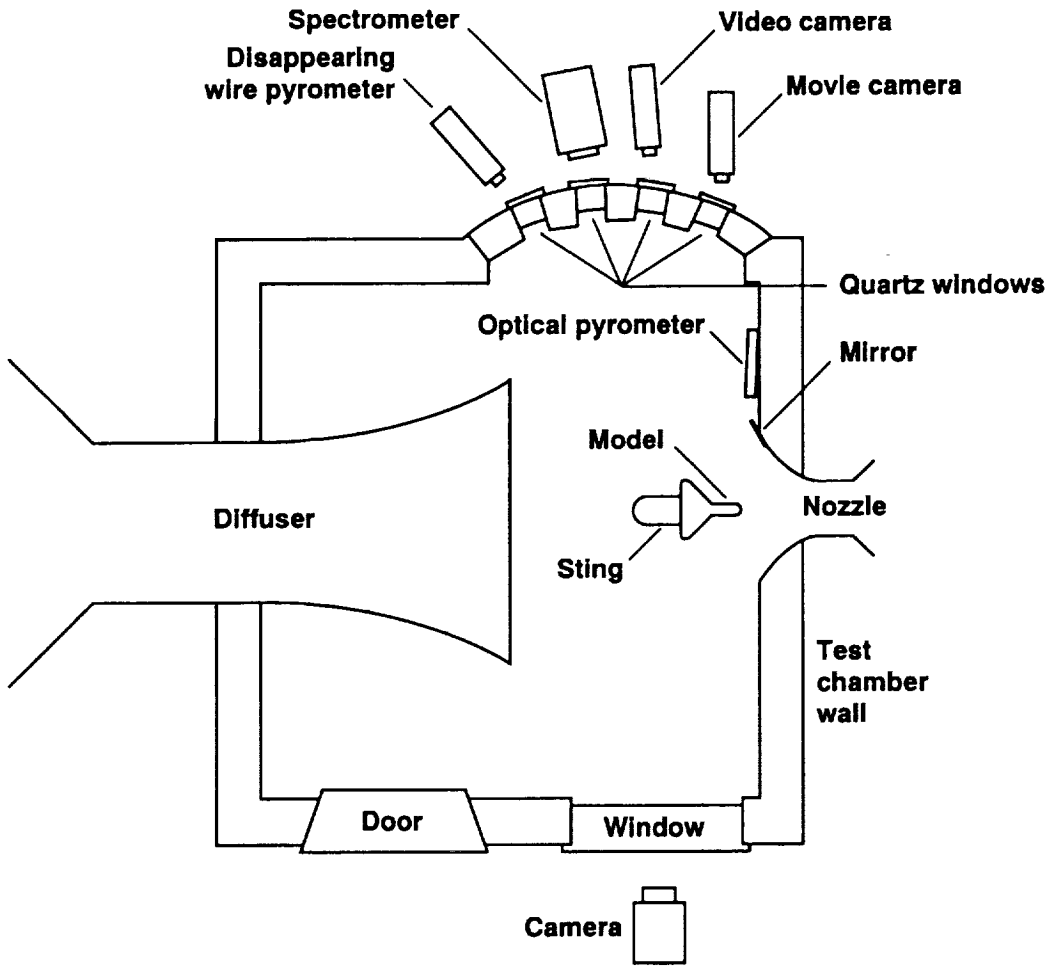

Figure 4. Instrumentation arrangement for LCA's arc-jet tests.

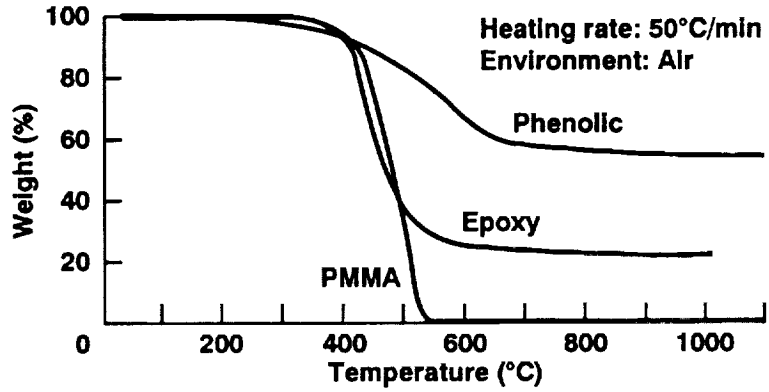

Figure 5. Thermogravimetric analysis of organic infiltrants. (a) Phenolic, (b) epoxy, (c) polymethylmethacrylate (pmma).

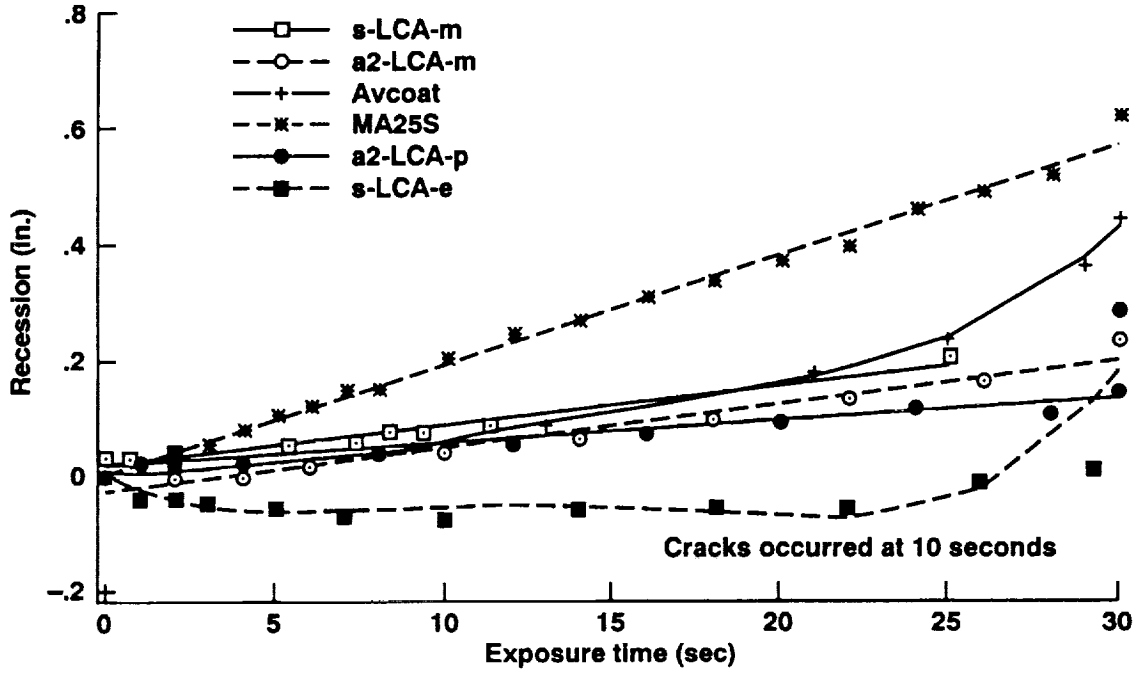

Figure 6. Fully dense LCA's stagnation point recession data at $\dot{q}$ = 830 Btu/ft^2-s and PT2 = 0.081 atm.

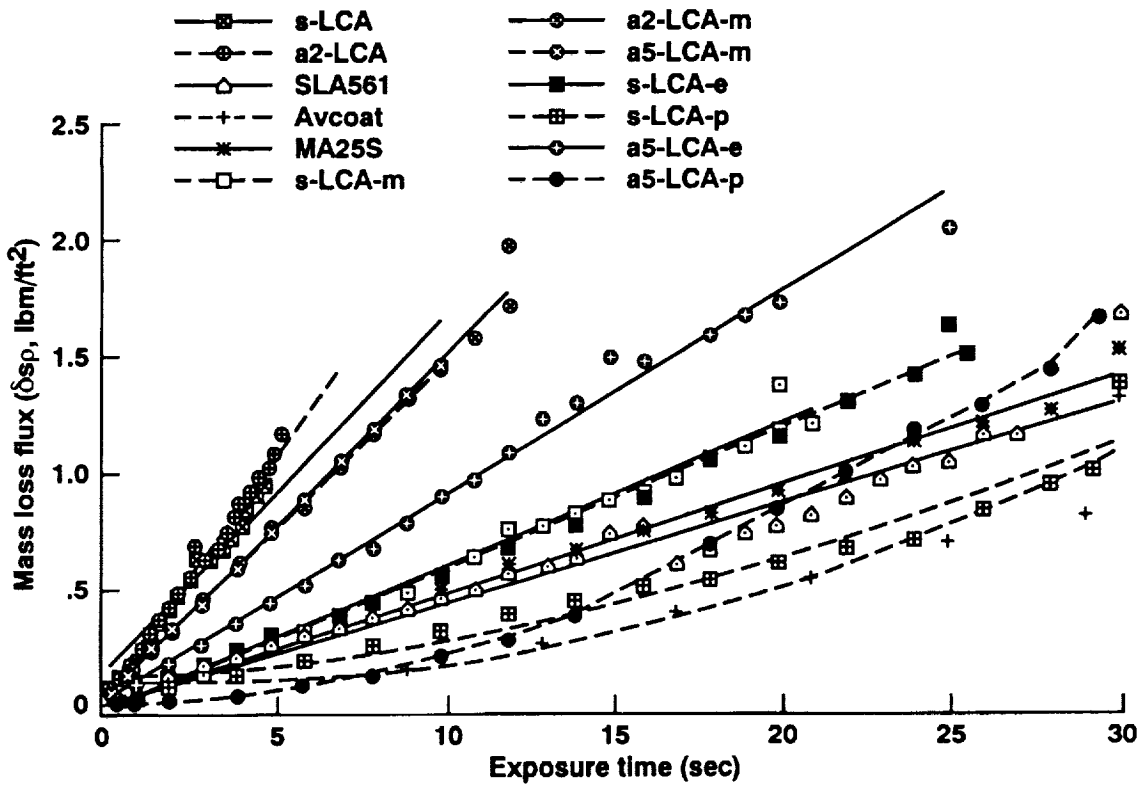

Figure 7. 60 MW arc-jet Phase I: stagnation point recession and mass loss flux at $\dot{q}$ = 830 Btu/ft^2-s and PT2 = 0.081 atm.

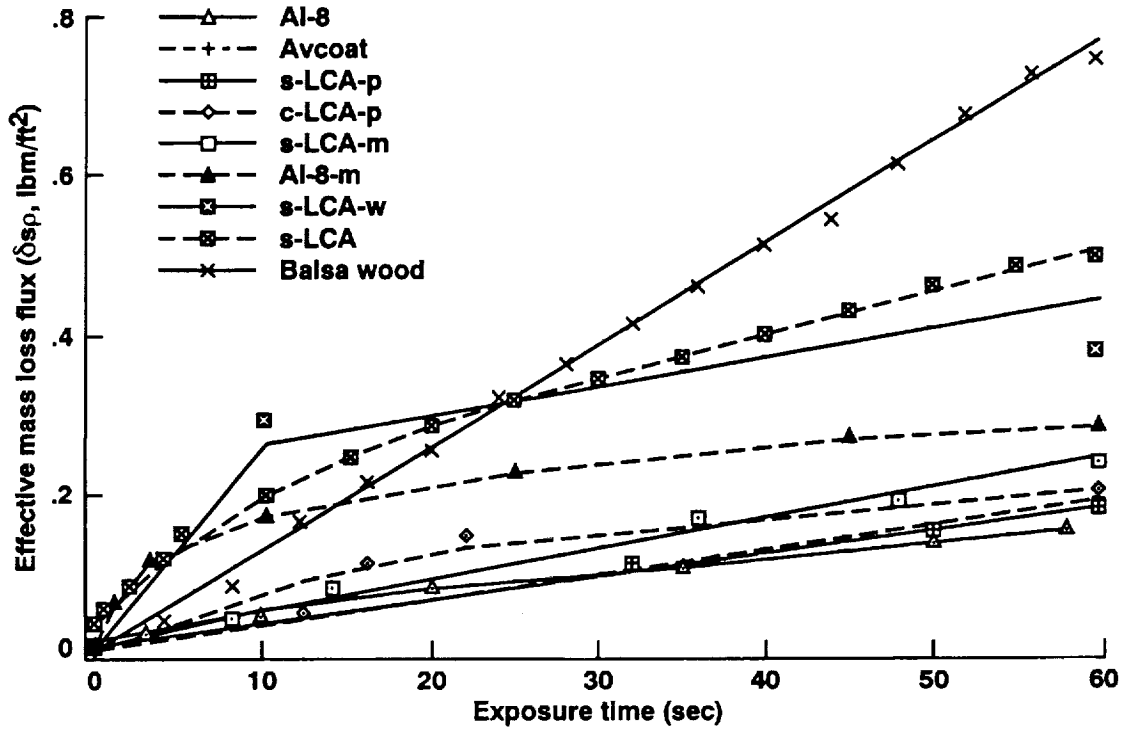

Figure 8. Effective mass loss flux based on recession data at $\dot{q}$ = 100 Btu/ft^2-s and PT2 = 0.012 atm.

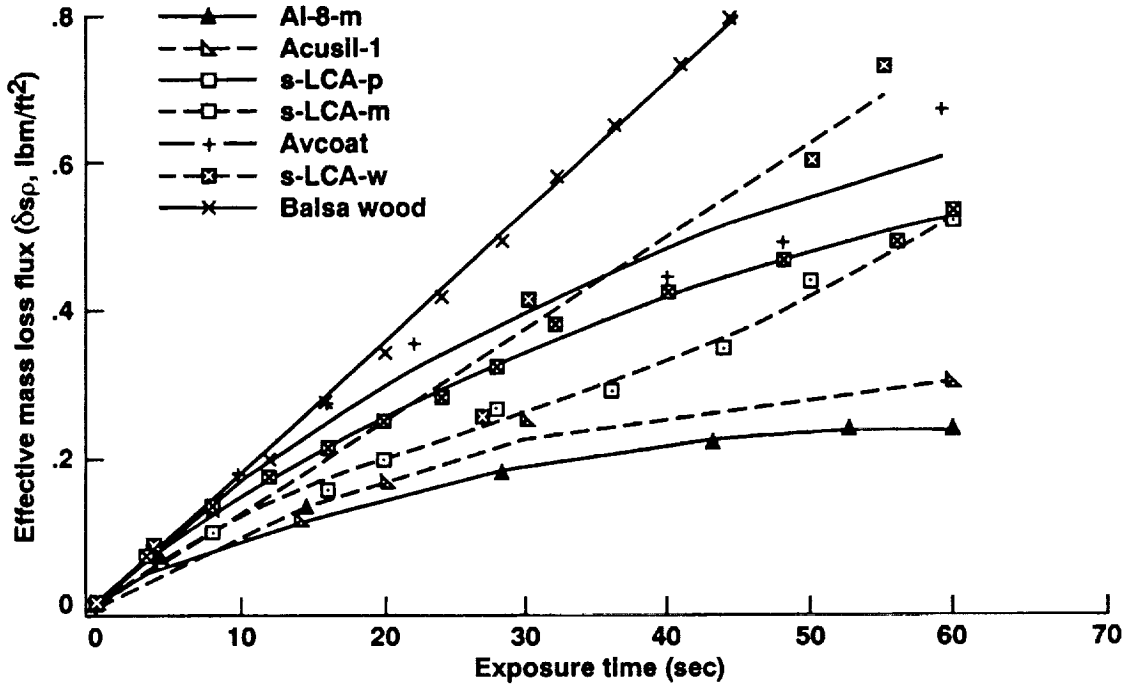

Figure 9. LCA's stagnation point recession and mass loss flux plots at $\dot{q}$ = 200 Btu/ft^2-s and PT2 = 0.025 atm.

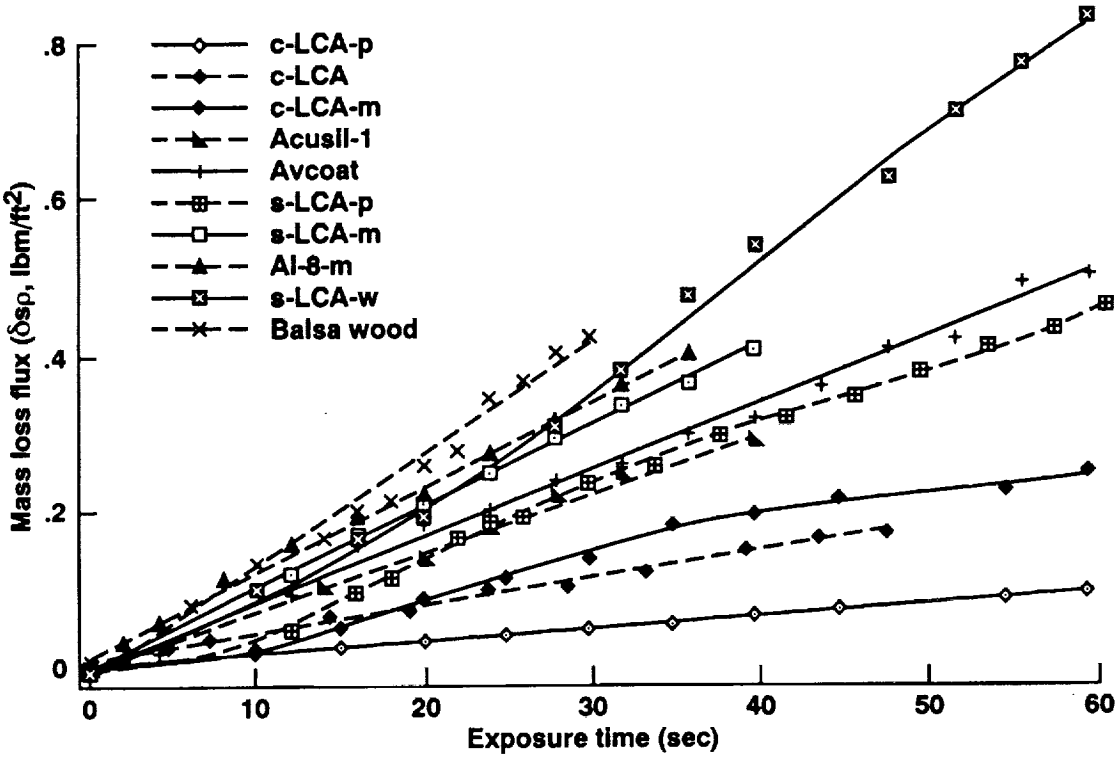

Figure 10. LCA's mass loss flux and recession plots at $\dot{q}$ = 400 Btu/ft^2-s and PT2 = 0.061 atm.

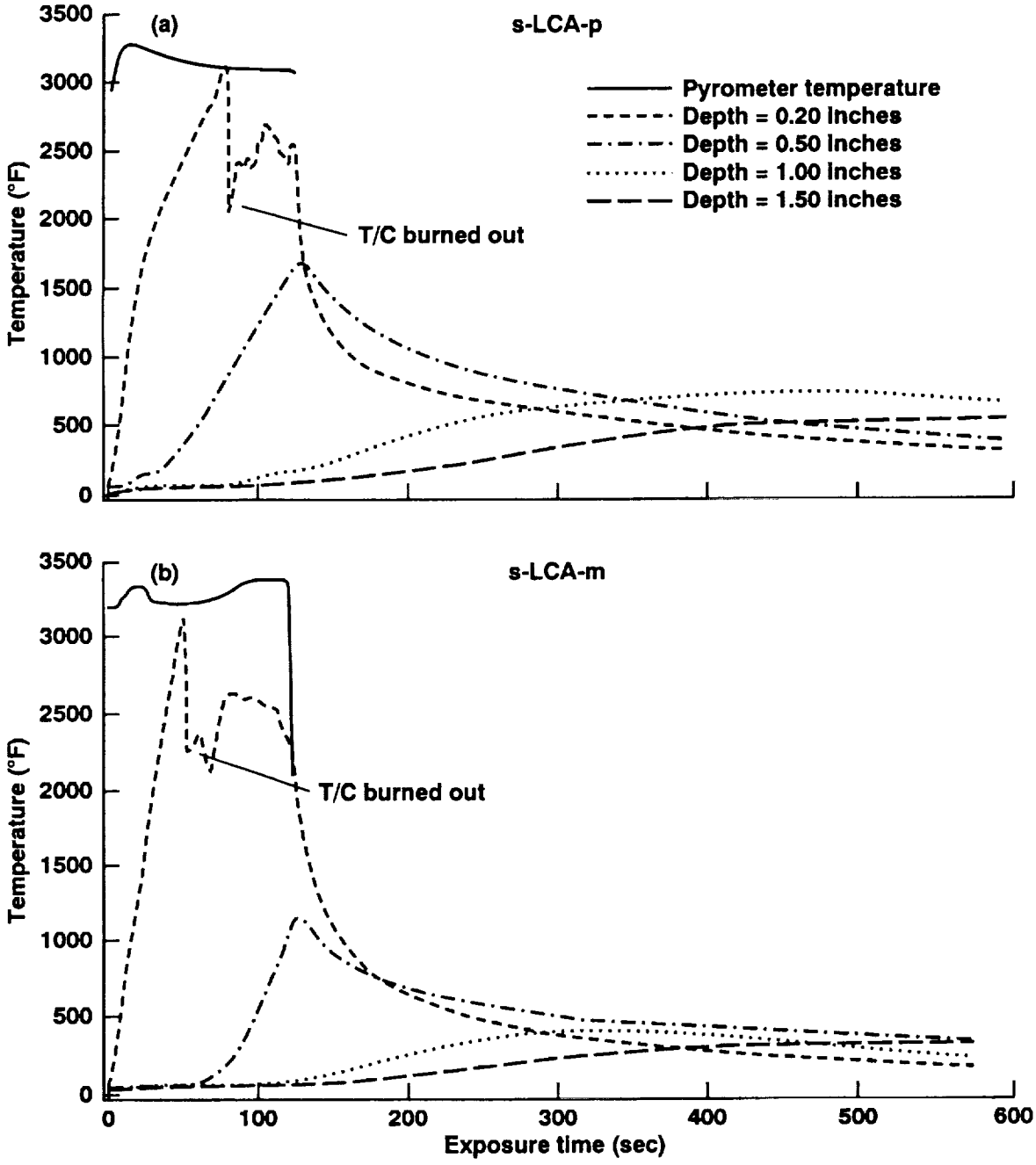

Figure 11. LCA's in-depth temperature profiles at $\dot{q}$ = 100 Btu/ft^2-s and PT2 = 0.018 atm. (a) LI-900/phenolic, (b) LI-900/pmma.

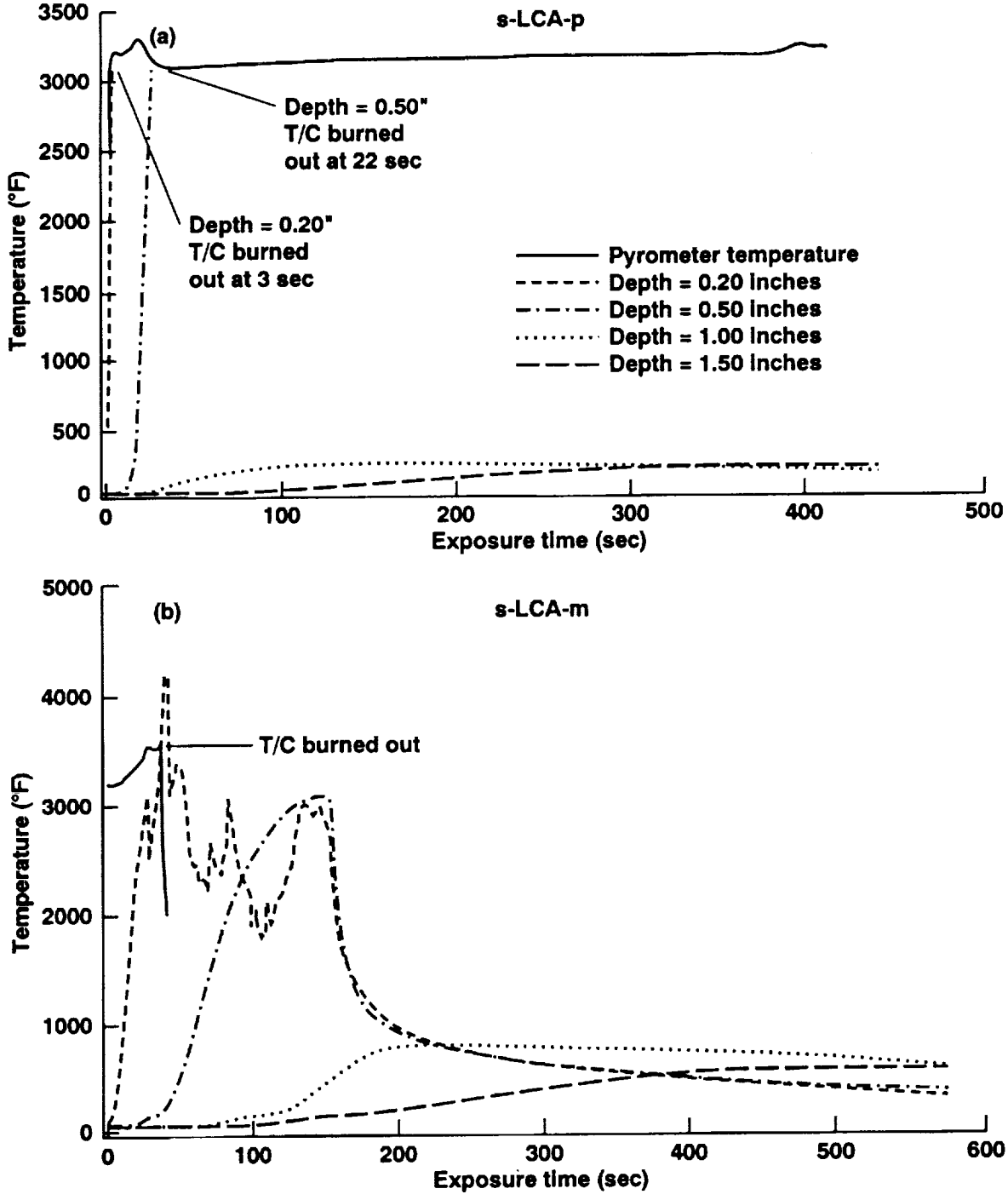

Figure 12. LCA's in-depth temperature profiles at $\dot{q}$ = 200 Btu/ft^2-s and PT2 = 0.025 atm. (a) LI-900/phenolic, (b) LI-900/pmma.

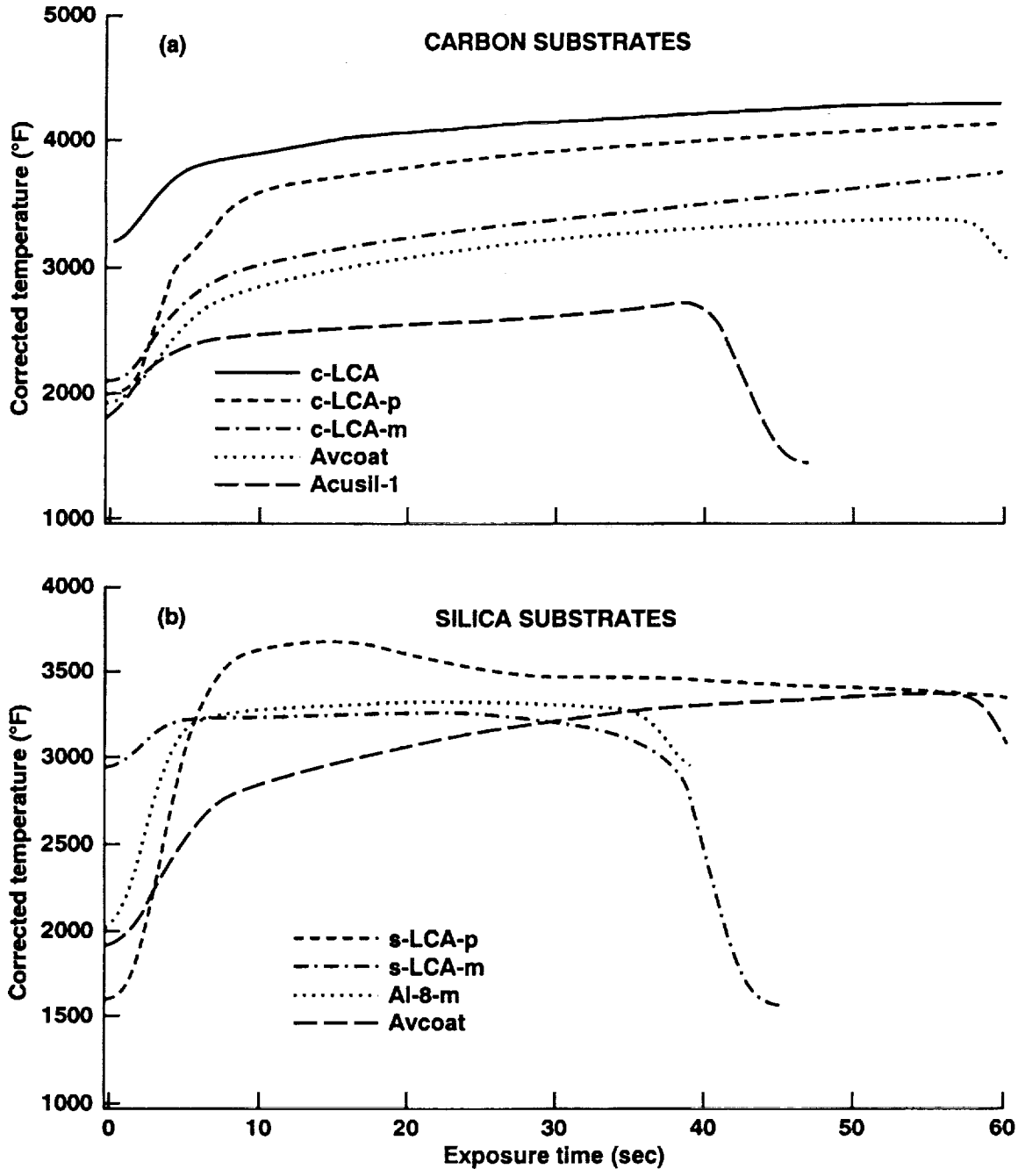

Figure 13. LCA's surface temperature plots obtained from an optical pyrometer at $\dot{q}$ = 400 Btu/ft^2-s and PT2 = 0.061 atm. (a) Carbon substrates, (b) silica substrates.

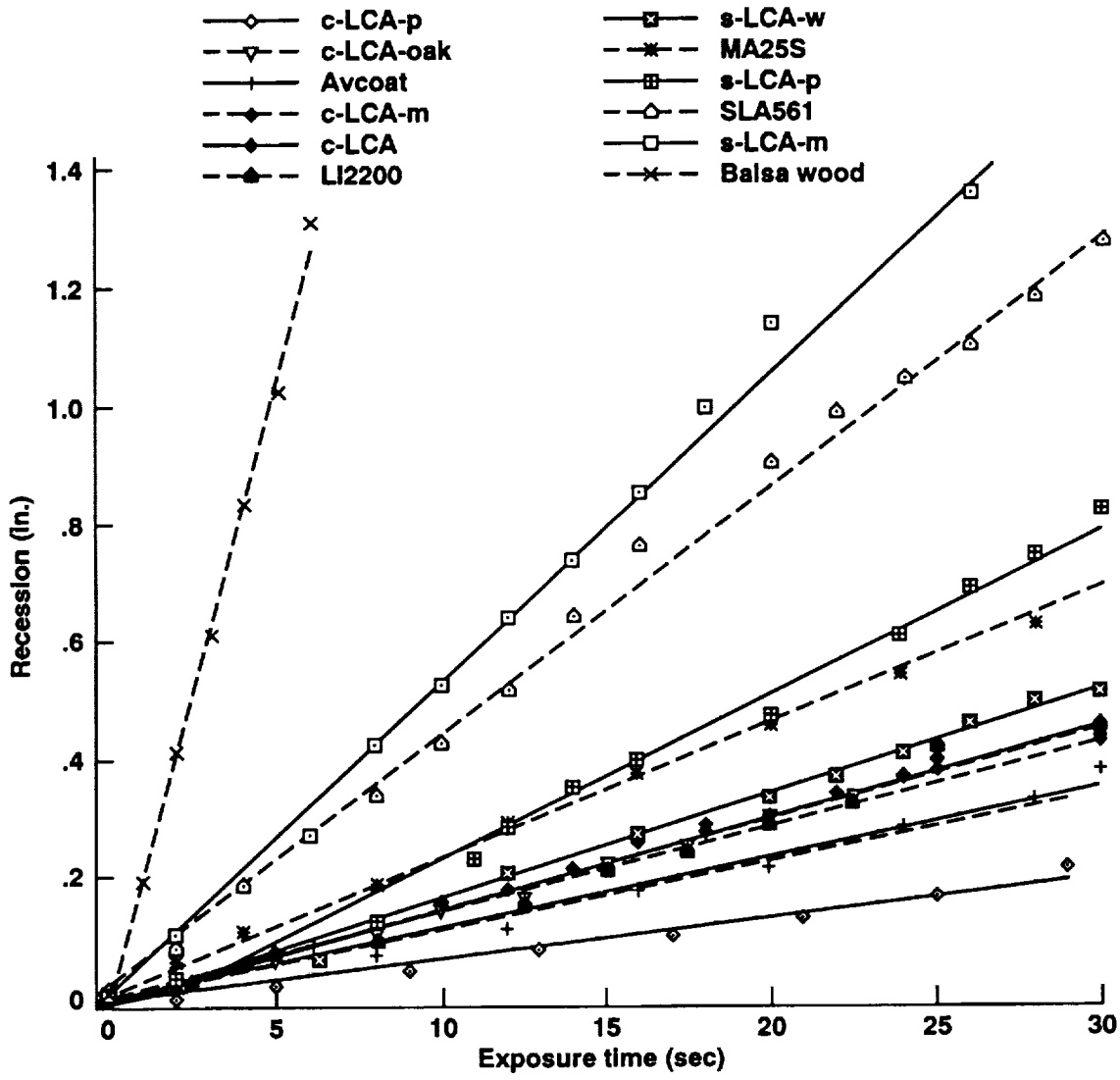

Figure 14. LCA's stagnation point recession data at $\dot{q}$ = 830 Btu/ft^2-s and PT2 = 0.081 atm.

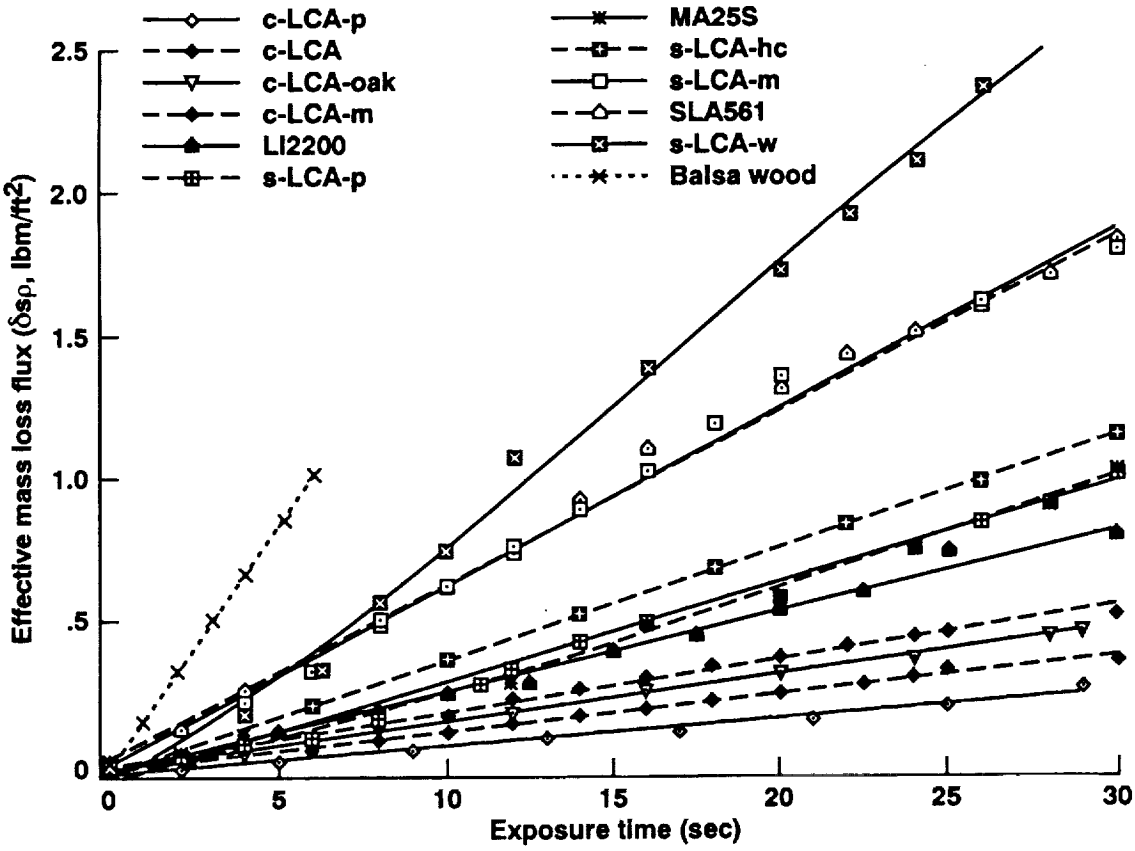

Figure 15. Effective mass loss flux based on recession data and virgin density at $\dot{q}$ = 830 Btu/ft^2-s and PT2 = 0.081 atm.

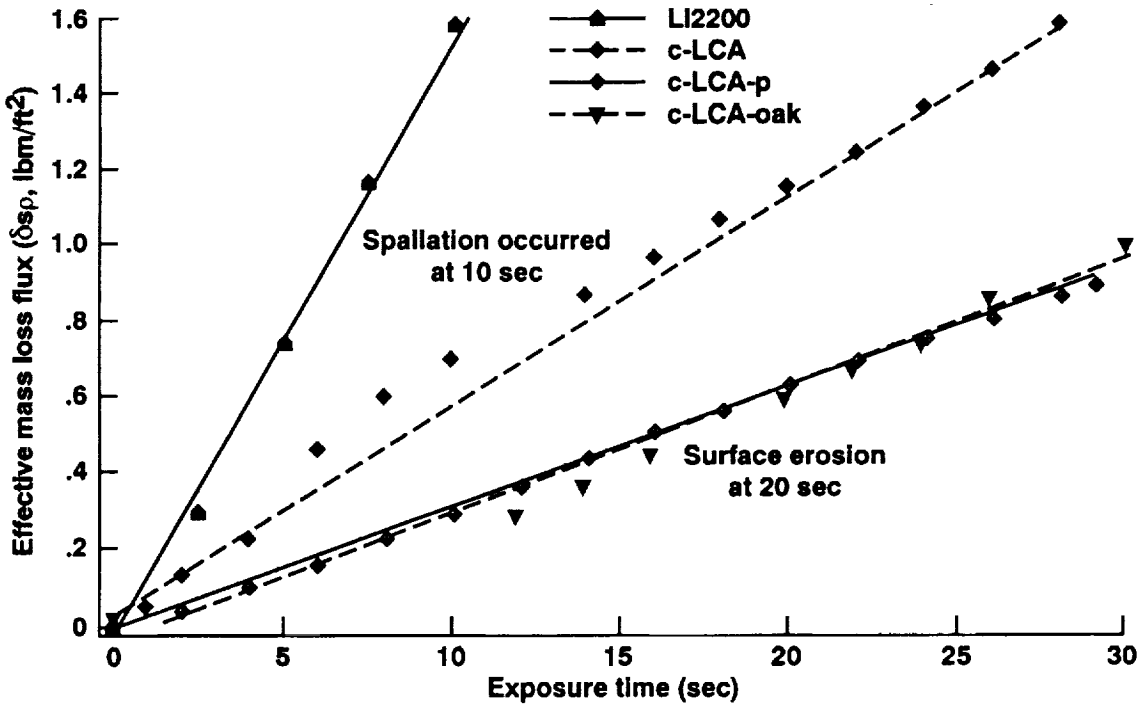

Figure 16. LCA's stagnation point recession data and mass loss flux at $\dot{q}$ = 1,440 Btu/ft^2-s and PT2 = 0.331 atm.

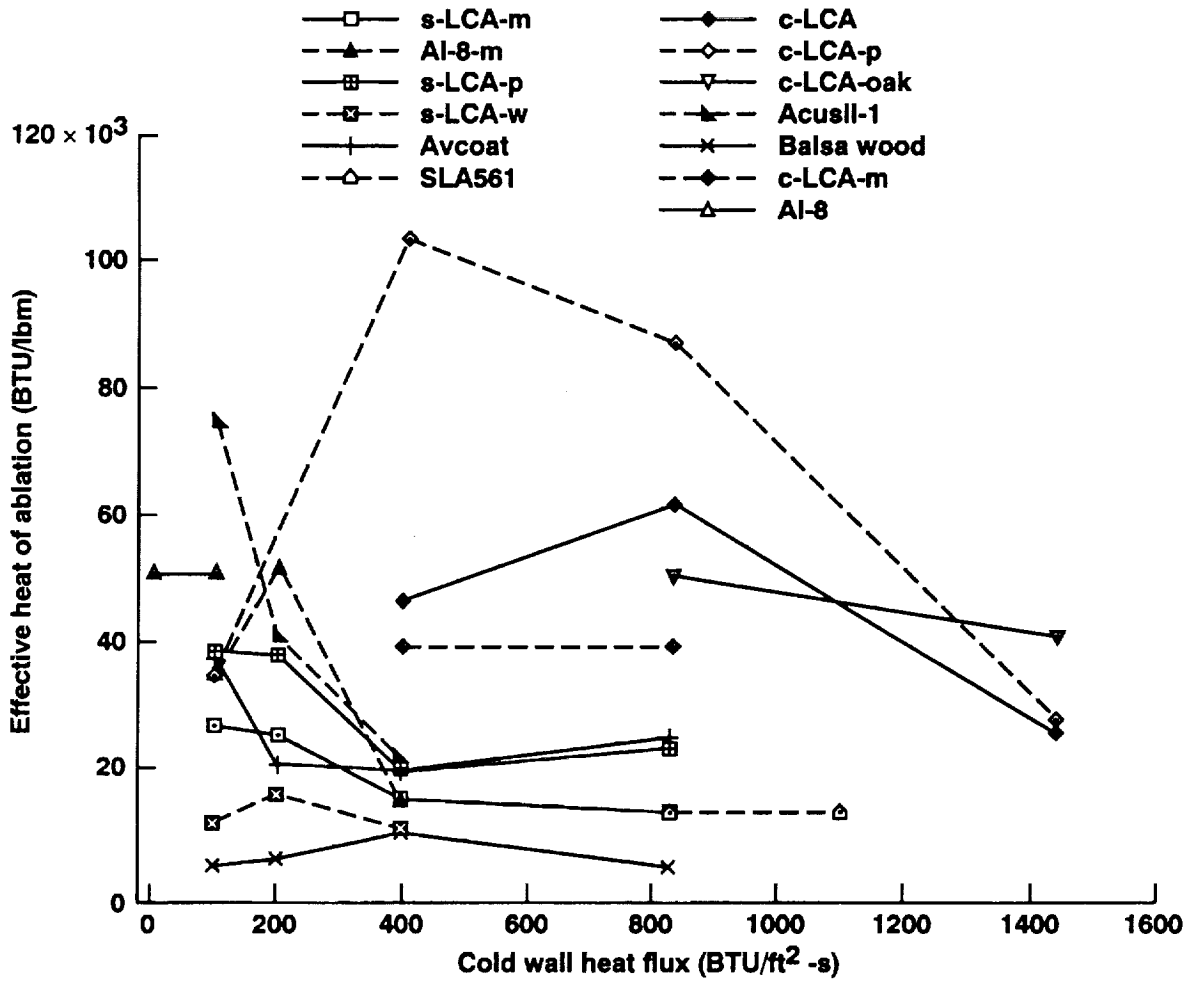

Figure 17. Mass efficiency plot of the lightweight ceramic ablators.

REPORT DOCUMENTATION PAGE

Form Approved
OMB No. 0704-0188

1. AGENCY USE ONLY *(Leave blank)*	2. REPORT DATE	3. REPORT TYPE AND DATES COVERED
	February 1994	Technical Memorandum

4. TITLE AND SUBTITLE

Development of Lightweight Ceramic Ablators and Arc-Jet Test Results

5. FUNDING NUMBERS

506-46-31

6. AUTHOR(S)

Huy K. Tran

7. PERFORMING ORGANIZATION NAME(S) AND ADDRESS(ES)

Ames Research Center
Moffett Field, CA 94035-1000

8. PERFORMING ORGANIZATION REPORT NUMBER

A-94017

9. SPONSORING/MONITORING AGENCY NAME(S) AND ADDRESS(ES)

National Aeronautics and Space Administration
Washington, DC 20546-0001

10. SPONSORING/MONITORING AGENCY REPORT NUMBER

NASA TM-108798

11. SUPPLEMENTARY NOTES

Point of Contact: Huy K. Tran, Ames Research Center, MS 234-1, Moffett Field, CA 94035-1000; (415) 604-0219

12a. DISTRIBUTION/AVAILABILITY STATEMENT

Unclassified — Unlimited
Subject Category 23

12b. DISTRIBUTION CODE

13. ABSTRACT ***(Maximum 200 words)***

Lightweight ceramic ablators (LCAs) were recently developed at Ames to investigate the use of low density fibrous substrates and organic resins as high temperature, high strength ablative heat shields. Unlike the traditional ablators, LCAs use porous ceramic/carbon fiber matrices as substrates for structural support, and polymeric resins as fillers. Several substrates and resins were selected for the initial studies, and the best performing candidates were further characterized.Three arc-jet tests were conducted to determine the LCA's thermal performance and ablation characteristics in a high enthalpy, hypersonic flow environment. Mass loss and recession measurements were obtained for each sample at post test, and the recession rates were determined from high speed motion films. Surface temperatures were also obtained from optical pyrometers.

14. SUBJECT TERMS	15. NUMBER OF PAGES
Ablators, Ceramic, Low density	28
	16. PRICE CODE: A03

17. SECURITY CLASSIFICATION OF REPORT	18. SECURITY CLASSIFICATION OF THIS PAGE	19. SECURITY CLASSIFICATION OF ABSTRACT	20. LIMITATION OF ABSTRACT
Unclassified	Unclassified		